Supplement of Hydrol. Earth Syst. Sci., 30, 3675–3695, 2026
https://doi.org/10.5194/hess-30-3675-2026-supplement

Hydrology and Earth System Sciences
Open Access
EGU

Supplement of

Satellite Data Rendered Irrigation using Penman–Monteith and SEBAL – sDRIPS for Surface Water Irrigation Optimization

Shahzaib Khan et al.

Correspondence to: Shahzaib Khan (skhan7@uw.edu)

Supplementary Information

S1. Creation of Configuration Files (Step 1):

The configuration files provide the essential information required for the sDRIPS system to tailor the advisory system to the specific needs of the user. There are three configuration files, namely the Script Config File, Crop Config File, and Command Area Config File. These files store necessary file paths, information about the crops grown in each command area, the dates for which the system must run, and other pertinent details. Below are the details of the functionality of each of the configuration files.

Script Config File: This file stores the path to the command area shapefile, the date for which the system is to be run, and whether the user wants to run the system for the current week, last week, or both. Furthermore, script configuration file holds Boolean statements ("True" or "False") to consider different modules (say percolation or precipitation forecast) into the analysis

Crop Config File: This configuration file stores the crop coefficient (Kc) values as a function of days. By default, it includes Kc values for several crops. Having a configuration file for Kc values gives users the flexibility to update Kc values as needed, especially with the introduction of high-yielding crops or when a cropping pattern needs to be simulated for changing climate conditions. Additionally, the simple structure of the file allows users to add new crops and drop existing crops for water management analysis.

Command Area Config File: This file is created based on user inputs and is automatically scaled to each command area. It includes data such as the planting date, crop type, and soil coefficient (default is 0.5) for each command area. This setup provides users with the flexibility to input specific values for each command area. Additionally, users can set default values that will be automatically applied to all command areas, simplifying the configuration process.

In cases where users do not have the command area shapefile, sDRIPS can iteratively generate buffer regions around each canal until it reaches the required serving area. This approach requires information on how much area each canal serves. The method back calculates the command area boundary based on the canal's serving capacity. While this method may not be entirely accurate, it provides a reasonably precise boundary to begin with.

S2. User Friendliness of sDRIPS

The sDRIPS system is designed to address the gaps identified in the current literature, as mentioned in section 1 of the study, by providing a user-friendly and customizable tool for analyzing various irrigation scenarios. The primary key features that enhance the usability of sDRIPS are as follows:

1. Ease of Use and Customization: sDRIPS employs configuration files that allow users to modify variables without altering the main script. To implement sDRIPS in a specific region, requirements are minimal, users need to have a Google Earth Engine (GEE) account and a Precipitation Processing System (PPS) account. Additionally, users must provide the canal network shapefiles, the command area of each

canal (recommended but optional), the types of crops to be included in the analysis, and the planting dates.

2. Debugging Support: sDRIPS supports debugging by logging detailed information at every step. This includes completion reports, error messages, and the corresponding line numbers, which assist users in identifying and resolving issues efficiently.

3. Real-Time Analysis Status: During the execution of its algorithms, sDRIPS displays a progress bar for each algorithm, along with an estimated time to completion allowing users to monitor the status of ongoing processes.

4. Low Computational Power: sDRIPS leverages the GEE cloud computing platform for core processes such as Penman-Monteith and SEBAL-based ET estimation, thereby eliminating the need for high-performance computing resources. This ensures that users can run the system effectively without requiring advanced computational infrastructure.

S3. Uncertainty Analysis

S3.1. Through changing input parameters

We conducted Monte Carlo simulations by perturbing the six key input parameters, listed in *Table S1*. Two methods of perturbation were employed:

1. Applying fixed percentage changes based on satellite retrieval uncertainty, and
2. Randomly sampling values within realistic bounds informed by observational variability and literature.

Both methods yielded similar results in terms of ET distribution, reinforcing the robustness of the uncertainty propagation approach. Here we have focused on the approach (a).

Table S1: Parameters perturbed in Monte Carlo Simulations

Sr. No	Parameter	Range
1	Normalized Difference Vegetation Index (NDVI)	±20% from estimated
2	Albedo	±20% from estimated
3	Leaf Area Index (LAI)	±20% from estimated
4	Surface Roughness	±20% from estimated
5	Aerodynamic Resistance	±20% from estimated
6	Emissivity	±20% from estimated

Using these perturbed inputs, we generated an ensemble of 1,000 Monte Carlo simulations over the selected command area, covering multiple timestamps throughout the study period. The relative spread of each

ensemble was calculated using equation S1, where Q_3 and Q_1 denote the 75th and 25th percentiles of the ET distribution, respectively. *Fig. S1* presents the boxplot of ET ensembles at a representative timestamp, demonstrating that the ensemble mean and median closely align with the deterministic (unperturbed) estimate for all time periods.

$$Realtive\ Spread = \frac{Q_3 - Q_1}{median} \quad S1$$

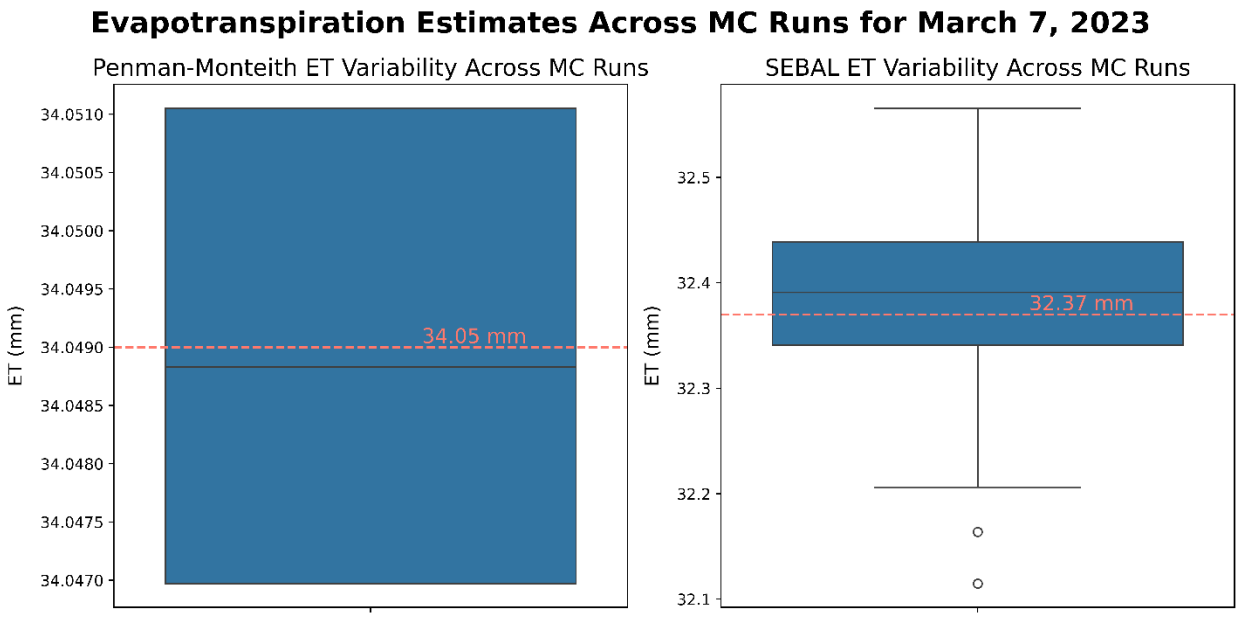

Fig. S1: Box plots for ET estimates across 1000 Monte Carlo Simulations.

This non-parametric measure of uncertainty (relative spread) allowed us to generalize the uncertainty bounds to other TBP command areas with similar agro-climatic conditions. The mean relative spread was used as a scaling factor for extending uncertainty estimates region wide. Subsequently, the upper and lower bounds of the ET estimates were derived using the equations S2 and S3, where ET_{det} is the deterministic or unperturbed estimate. The final uncertainty-propagated estimates for net water requirements are summarized in Table S2 and visualized in Fig. S2.

$$Lower\ Bound = ET_{det} - \frac{Relative\ Spread \times ET_{det}}{2} \quad S2$$

$$Upper\ Bound = ET_{det} + \frac{Relative\ Spread \times ET_{det}}{2} \quad S3$$

Furthermore, the deterministic SEBAL-derived ET values were compared to the ensemble mean generated through the Monte Carlo simulations. Specifically, we computed the normalized deviation of the deterministic estimate from the ensemble mean using equation S4, where SEBAL ET_{det} is the deterministic SEBAL estimate and $Ensemble_{std}$ is the standard deviation of the ensemble.

$$Normalized\ Deviation = \frac{SEBAL\ ET_{\det} - Ensemble_{mean}}{Ensemble_{std}} \times 100 \quad S4$$

The mean normalized deviation over the operational period of the Teesta Barrage Project (January–April) was found to be 8.6%, indicating that the deterministic SEBAL values deviated by an average of 8.6% from the ensemble mean. This indicates that, on average, deterministic SEBAL estimates deviated by 8.6% from the ensemble mean, offering a quantitative measure of uncertainty. The relatively low deviation supports the validity of using deterministic SEBAL outputs as central estimates and justifies the scaling of results to other TBP command areas with similar climatic conditions.

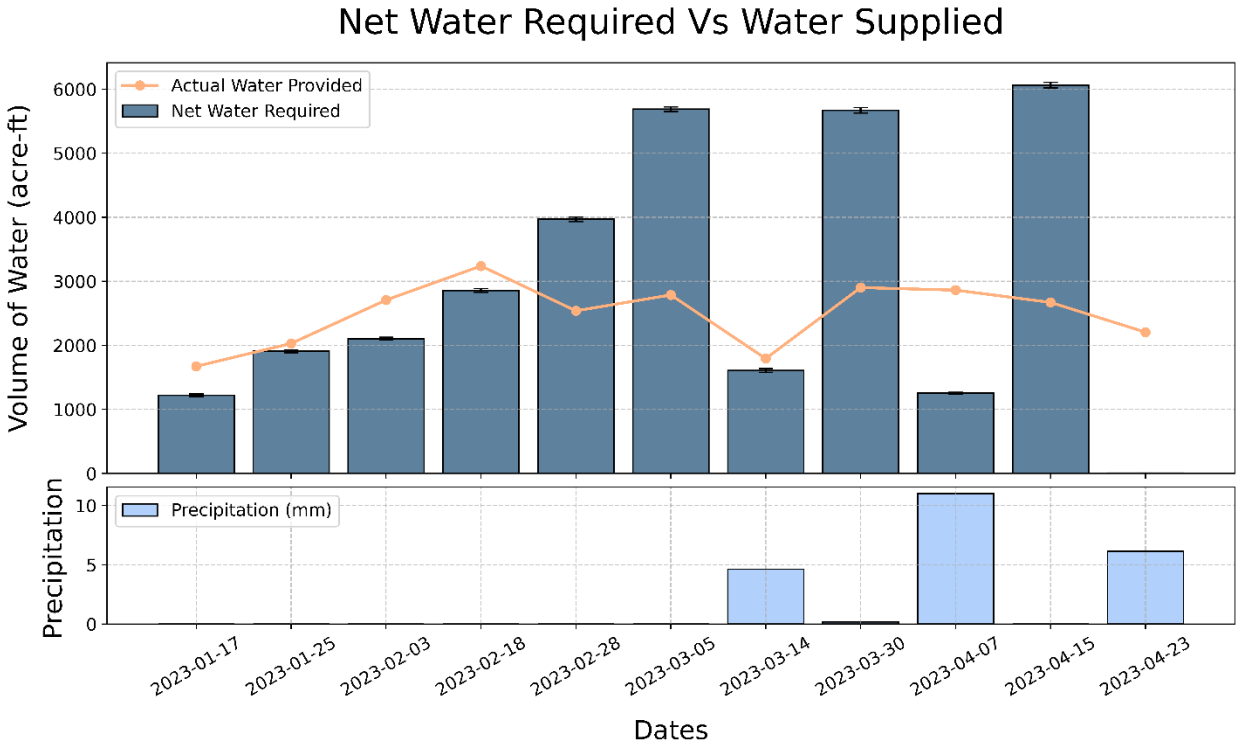

Fig. S2: Timeseries of net water required by TBP along with the uncertainty bounds vs amount of water supplied to TBP.

Table S2: Net water required with uncertainty bounds.

Date	Net Water Required (acre-feet) (Lower Bound)	Net Water Required (acre-feet)	Net Water Required (acre-feet) (Upper Bound)	Bounds in Percentage (%)
2023-01-17	1198.45	1220.84	1243.22	1.83
2023-01-25	1887.65	1910.08	1932.50	1.17
2023-02-03	2083.92	2105.58	2127.25	1.03
2023-02-18	2830.56	2859.13	2887.71	1.00
2023-02-28	3936.99	3971.39	4005.79	0.87
2023-03-05	5656.08	5691.31	5726.54	0.62
2023-03-14	1578.56	1607.07	1635.74	1.77
2023-03-30	5630.56	5672.99	5715.42	0.75
2023-04-07	1242.52	1254.53	1266.54	0.96
2023-04-14	6024.52	6067.50	6110.48	0.71
2023-04-23	7.10	7.64	8.18	7.05

S3.2. Through Sensitivity Analysis:

Sensitivity analysis focusing on two key drivers of evapotranspiration - air temperature and precipitation was conducted. According to (Zhang et al., 2025) these parameters significantly influence evapotranspiration depending on the climatic regime. The analysis evaluates how uncertainties in these inputs impact evapotranspiration estimates and, consequently, the net water requirements.

1. Sensitivity to Air Temperature: We perturbed the air temperature by ±1°C and analyzed the response in both Penman-Monteith ET (potential ET under optimal water conditions) and SEBAL ET (actual ET under water stress). Fig. S3 illustrates the results, where the upper panel presents the time series of seven-day cumulative Penman-Monteith evapotranspiration (mean of the region) and the lower panel displays the SEBAL evapotranspiration under the same perturbation. The expected trend is observed, with an increase in air temperature leading to a corresponding increase in evapotranspiration and a decrease in temperature resulting in lower evapotranspiration estimates. Furthermore, the temporal variation in evapotranspiration aligns with the crop growth cycle - initial, development, and harvesting phases. In terms of magnitude, a ±1°C change in air temperature leads to an approximate change of 1.4 mm in Penman-Monteith evapotranspiration and around 1 mm in SEBAL evapotranspiration, indicating that potential evapotranspiration under ideal conditions is

slightly more sensitive to temperature variations compared to actual evapotranspiration under the water-stressed conditions.

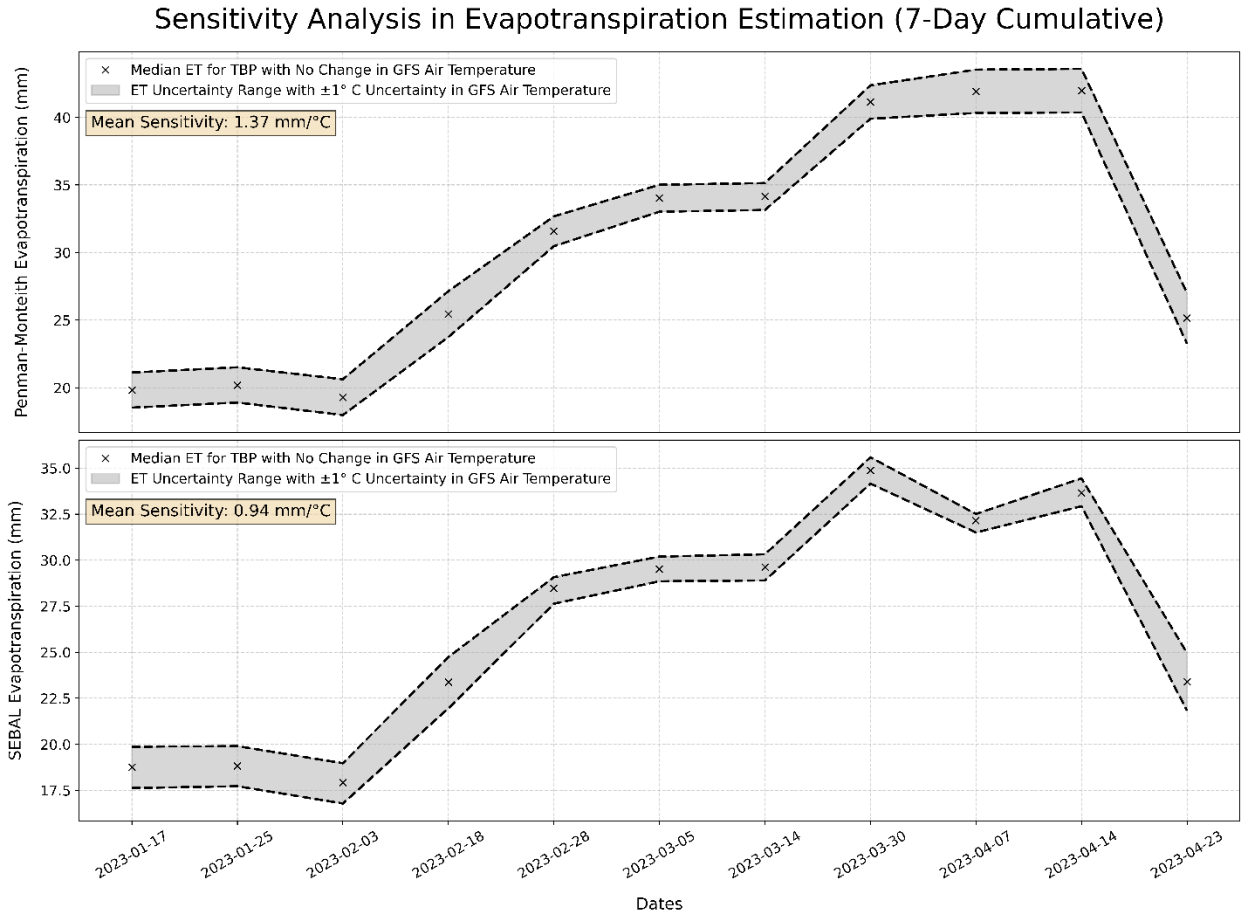

Fig. S3: Sensitivity Analysis in Evapotranspiration Estimation

To further understand the implications of this variation, we assessed how these changes in evapotranspiration translate into changes in net water requirement. Fig. S4 presents the sensitivity analysis in this context, consisting of two panels: the upper panel illustrates the volume of water required and the amount provided by in-situ supply, while the lower panel depicts the contribution of precipitation. The results indicate that a ±1°C change in air temperature leads to an approximately 0.4 million m³ variation in net water requirement, emphasizing the role of temperature fluctuations in water demand estimation.

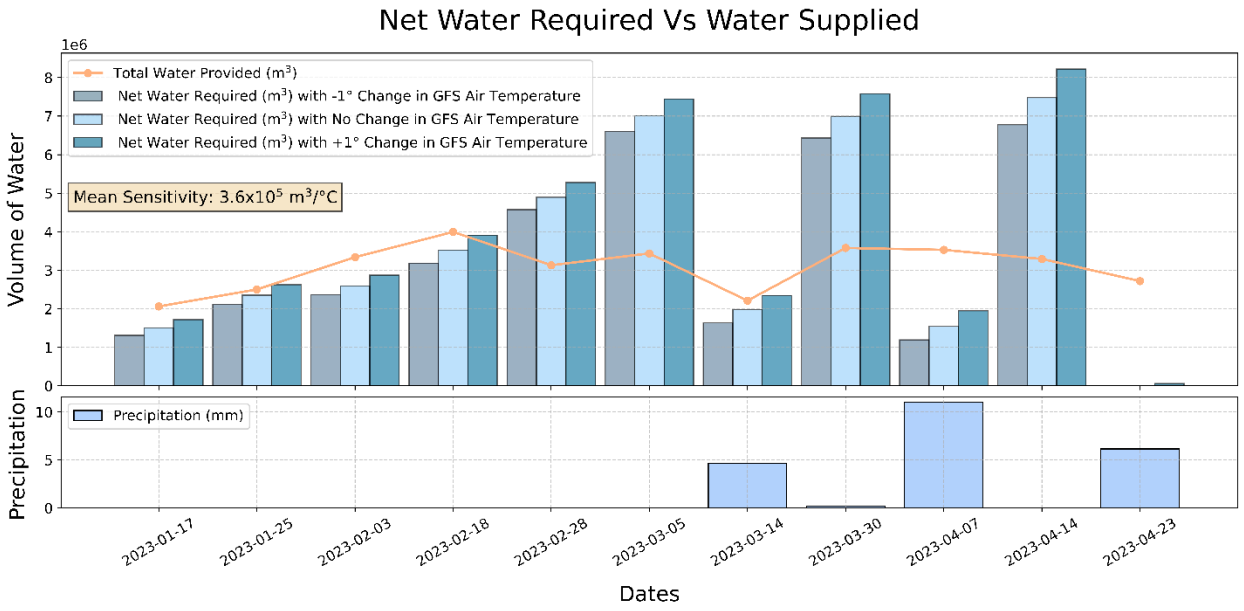

Fig. S4: Sensitivity Analysis for Net Water Required w.r.t. Change in Air Temperature

2. Sensitivity to precipitation: Given its direct role in balancing water demand, we investigated the impact of a ±1 mm change in precipitation over the entire Teesta Barrage Project (TBP) region. Fig. S5 presents this analysis, and the results indicate that a 1 mm increase in precipitation reduces the net water requirement by approximately 1 million m³, demonstrating a more pronounced impact than air temperature fluctuations. This highlights the significance of precipitation uncertainty, as even minor deviations in precipitation estimates can substantially alter water demand calculations.

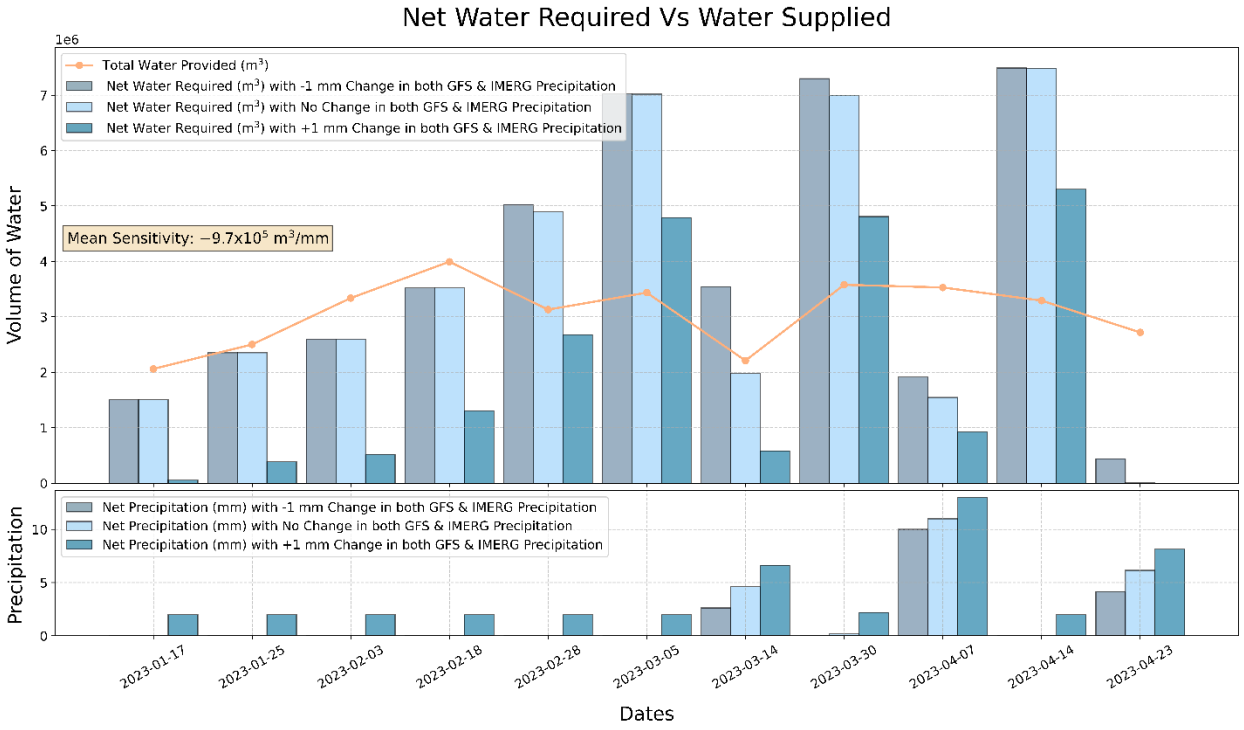

Fig. S5: Sensitivity Analysis for Net Water Required w.r.t. Change in Precipitation

A comparison of these two factors suggests that in a hypothetical scenario, if water managers had control over modifying either air temperature or precipitation, increasing precipitation by 1 mm over entire TBP would be more beneficial than reducing air temperature by 1°C over entire TBP, as the former leads to greater water savings. This underscores the importance of accurate precipitation forecasting in improving water resource management and planning. Overall, our sensitivity analysis highlights the extent to which uncertainties in key meteorological inputs influence water demand estimations, emphasizing the need for robust data sources and improved forecasting methods to enhance the reliability of net water requirement assessments.

S4. References

Zhang, H., Wang, G., Li, S., and Cabral, P.: Understanding Evapotranspiration Driving Mechanisms in China With Explainable Machine Learning Algorithms, International Journal of Climatology, https://doi.org/10.1002/joc.8774, 2025.